Journal of Instrumentation

SISSA

PAPER • OPEN ACCESS

Track reconstruction of particle interactions in long crystals with large bending

To cite this article: R. Rossi *et al* 2021 *JINST* **16** P05017

Published by IOP Publishing for Sissa Medialab

Received: *December 3, 2020*
Revised: *February 4, 2021*
Accepted: *February 11, 2021*
Published: *May 31, 2021*

Track reconstruction of particle interactions in long crystals with large bending

R. Rossi,[*,a] **L.S. Esposito,**[a] **M. Garattini,**[a,b] **T.O. James,**[b] **M. Pesaresi,**[b] **G. Hall**[b] **and W. Scandale**[a,b]

[a] *European Organization for Nuclear Research CERN, Geneva, Switzerland*
[b] *Blackett Laboratory, Imperial College, London SW7 2AZ, U.K.*

E-mail: Roberto.Rossi@cern.ch

Abstract: The possibility to deflect hadron beams precisely through angles of multi-mrad is important for several future applications, and magnets are not suitable for this purpose. Crystal channeling provides a means to do this, but is not well studied for such deflections. Measurements of the interactions of charged particles with several cm long crystals with large bending have been obtained by the UA9 collaboration. These crystals have a bending 100 times larger and a length along the beam direction up to 40 times longer than the ones presently used by UA9 in the CERN accelerators. To assess their properties and quality, the crystals have been investigated in the CERN North Area with a Super Proton Synchrotron beam of mixed hadrons at 180 GeV. The UA9 tracking telescope has been adapted to collect data with these particular crystals. A new track reconstruction method is described which was required to obtain the results reported, and has been used in the present study to validate the methodology, so that detailed assessments of future systems can be made.

Keywords: Particle tracking detectors; Analysis and statistical methods; Data processing methods

*Corresponding author.

https://doi.org/10.1088/1748-0221/16/05/P05017

2021 JINST 16 P05017

Contents

1 Introduction

Planar channeling appears in crystals due to the electrostatic potential well which is generated by nuclei in two adjacent crystalline planes and encountered by charged particles traveling in the material. The necessary condition is for the particles to have a transverse momentum lower than the potential well height [1]. This condition can be imposed on the impact angle of the particles entering the crystal, defining a critical angle θ_c above which channeling is not achieved. With this premise, bent crystals can be exploited to steer a beam of charged particles. A crystal of length l along the beam direction is given a radius of curvature R and a bending angle $\theta_b = l/R$. The bending produces a deformation of the potential well, at the same time reducing the θ_c value. Below a critical value of the radius R_c [1] the well is no longer observed and channeling cannot be achieved. Both the critical values θ_c and R_c depend on the crystal atomic number and the particle momentum. Bent crystals have been recently used for various methods of particle beam manipulation. The most successful achievement has been the demonstration of hadron beam collimation using crystals in the LHC [2].

For future fixed target experiments at the LHC, bent crystals have been proposed as both halo extraction devices and to impart a spin precession to short-lived particles traveling along the crystal in channeling mode [3, 4]. Crystals for such applications are required to have a bending angle in the range of tens of mrad. Compared to present day LHC and SPS crystals used for collimation studies [2, 5], the required bending is 100 times larger. Given that R must remain well above the critical value R_c to achieve a sufficient channeling efficiency at the LHC energy [6], the crystals need to be manufactured with a length of a few cm, in contrast to the present length of a few mm. A few preliminary measurements of crystals with bending angles of several mrad were made in the early 1990s [7] but the technologies of crystal (preparation, bending and mounting) and the

2021 JINST 16 P05017

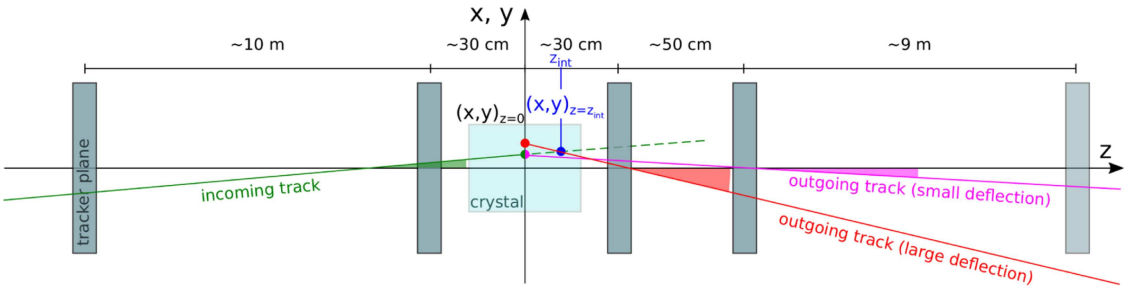

Figure 1. Tracker telescope layout. Silicon tracker planes (gray boxes) are shown, where the crystal (light blue box) is placed at the center of the reference system. Distances between consecutive elements are shown. Incoming (green line and angle) and outgoing (small deflection in magenta line and angle, large deflection in red line and angle) tracks are shown. The different z-vertex interaction points are highlighted for small and large deflection angles. In the latter case, the four-plane configuration needs to be used.

experimental apparatus have been revised since that time and, as this report will show, it is possible to acquire very large data sets quickly, improving the precision of the measurements.

2 Experimental layout

An extraction line is available from the CERN SPS to direct the beam toward the North Area that houses several experimental areas. The H8 line can be optimized to achieve a micro-beam (small beam divergence and spot size) suitable for crystal measurements. An area is adapted and dedicated to UA9 crystal measurements at the most upstream available position on the H8 line. To reduce the interaction of beam particles with air, the tracker stations are installed where segments of vacuum beam pipes are removed to house them. The particular requirements of UA9 are satisfied in this special environment, renouncing to a certain level of flexibility of the experimental setup. The reference frame is identified with its origin at the crystal position and the beam direction along the z-axis, as shown in figure 1.

A tracking detector telescope [8–10] is used to reconstruct particle beam trajectories before and after the interaction with a crystal mounted on a goniometer. The tracker is composed of five stations (or planes) each hosting a pair of silicon strip sensors, mounted perpendicular to each other to resolve the particle hit in both the horizontal and vertical directions. The active area of each station is 3.8×3.8 cm^2. In its standard configuration, the incoming and outgoing arms are arranged to have a length of about 10 m on either side of the crystal (figure 1). The incoming arm is composed of two tracker stations, while the outgoing one consists of three stations. The longest vacuum pipe sections are in between the two arms: between the first and second plane and between the fourth and fifth plane. Given the dimensions of the active area and the lever arm of the outgoing section, the maximum deflection measurable with this arrangement is ≈2.5–3.5 mrad.

To measure crystals with bending angles larger than these values, one could reduce the outgoing lever arm. As stated, the space between station four and five is occupied by a vacuum pipe; thus, to measure the outgoing tracks, only stations three and four are used. The limited space available

2021 JINST 16 P05017

Table 1. Telescope configurations used, showing the distance from the preceding layer. In the text, as in figure 1, the crystal position corresponds to the origin of the coordinate system.

Station	Alignment Δz (cm)	Sample 1 Δz (cm)	Sample 2 Δz (cm)	Sample 3 Δz (cm)
Station 1	0	0	0	0
Station 2	923.3	943.4	915	941.8
Crystal	70	30.5	65	25.1
Station 3	33.1	38.7	29.1	16.4
Station 4	36.5	44.5	54.7	54.1
Station 5	1025.4	1005.5	1033.1	1063.3

between the crystal and plane four position, due to the fixed position of the vacuum pipes in the incoming and outgoing arm, allows a maximum lever arm of ≈60 cm. This new layout requires the reconstruction algorithm to use only four planes instead of the standard five. In the next sections, a comparison between these so called 5-plane and 4-plane reconstruction methods is described.

The crystals are installed on a high precision movement stage. This stage is composed of different actuators, notably a linear actuator, to move the crystal in and out of the beam line along the x-axis, and a rotational actuator, used to modify the relative orientation of the crystal to the beam line, again along the horizontal direction. Given the layout of the movement stage, the crystals are installed to deflect the beam particles in the horizontal plane. For this reason, the analysis presented in the paper is mainly focused on the xz-plane. Nevertheless, all the results and conclusions for effects that are equivalent on the yz-plane (like multiple Coulomb scattering (MCS) when evaluating the tracker resolution) have been checked during the study.

In this paper two crystals with the same length (8 cm) but with a different bending angle (≈3 mrad and ≈12 mrad), and one shorter (2.5 cm), but with comparable bending (≈2.5 mrad), were selected for this study and identified as sample 1, sample 2 and sample 3, respectively. Also a run without crystals, known as a tracker alignment run, but with a different tracker configuration with respect to the sample measurements, is used to compare the particle track reconstruction methods. The different configurations of the telescope used for the measurements presented in the paper are listed in table 1, and referred to in the plots which follow.

3 Particle tracking

The standard particle tracking is based on an algorithm that takes into account several parameters, as described in detail in [10]. The reconstruction is optimized by means of alignment runs recorded without the crystal in the path of the beam. These runs contain straight tracks for both arms of the tracker and allow to adjust the relative alignment of the tracker stations in the transverse plane with respect to the beam direction. Also, the tracker resolution, defined as the standard deviation of the distribution of the difference of the incoming and outgoing track angle, can be measured.

2021 JINST 16 P05017

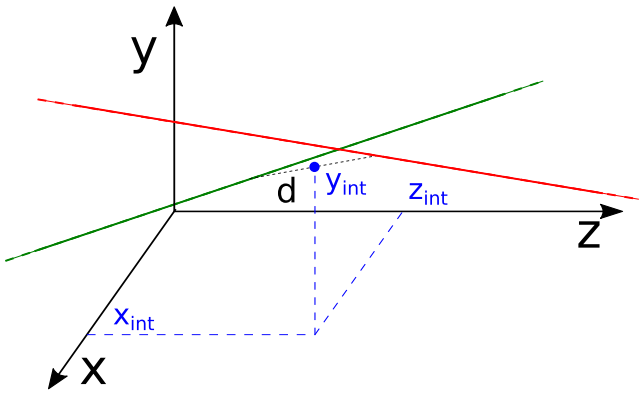

Figure 2. Schematic concept for 3D reconstruction of the intersection point (x_{int}, y_{int}, z_{int}) of two skew lines in Euclidean space. The midpoint of the minimum distance segment connecting the two lines is used as interaction vertex.

This value is influenced by multiple Coulomb scattering (MCS) due to the interactions of particles with tracker planes, pipe windows, and air.

The tracks recorded during crystal measurements are selected from a χ^2 distribution, based on the constraint that outgoing and incoming tracks have an interaction vertex at the crystal entry face, which corresponds to $z = 0$ in the reference system of the telescope. This method was used since 2012, demonstrating the reliability of tracker performance with different hadron and ion beams, and allowing more than ~300 crystal measurements in H8. Crystals for LHC and SPS are a few mm long; hence, the assumption of a point-like interaction vertex is appropriate.

For crystals longer than about 1 cm, this assumption is not valid. Due to the larger crystal length, the effective vertex position is located at a different depth within the crystal, depending on the deflection angle.[1] The approach used to solve this problem was to separate and treat independently the incoming and outgoing tracks, for every single event. A post-reconstruction algorithm was then applied to evaluate the longitudinal vertex position for each event in the three-dimensional reference frame used for track reconstruction. The outgoing and incoming track parameters are defined by two skew lines. The interaction vertex for each event is evaluated as the midpoint of the shortest segment connecting the two skew lines, as shown in figure 2. This method does not allow a χ^2 selection in the track reconstruction because only two points are available for each track. Also removing the constraint on the interaction vertex longitudinal position makes it possible to study the MCS contribution to the tracker transverse spatial resolution, which is not possible with the 5-plane configuration (where the constraint of a common interaction vertex for incoming and outgoing tracks is in place).

It is worth noting that the reconstructed longitudinal vertex distribution is very wide, especially for slightly deflected particles. The effect is due to the precision of estimating the longitudinal vertex when incoming and outgoing tracks have similar directions. In particular, particles that

[1] The trajectory of a channeled particle in a bent crystal should be quasi-circular, with deviations from coherent (e.g. volume reflection) or incoherent (multiple scattering) interactions with the atomic lattice in some cases. Hence the circular trajectory can easily be treated from simple geometric considerations as a deflection at one point since the reconstruction involves only the angle of incidence and the exit angle.

2021 JINST 16 P05017

travel through the volume of the crystal and experience only MCS have small deflections, compared to ones that experience a large deflection due to a channeling interaction. Channeled particles show a sharp z-vertex distribution, which can be used to select the crystal volume in the longitudinal beam direction, as will be shown in section 5. The characteristics of particles that are not bent or deflected by the crystal were also studied, including the RMS in both angular deflection and horizontal spatial displacement (the difference between the entry and exit points) due to the MCS interactions with the crystal in its amorphous orientation. This is essential in a bent crystal investigation because both straight and deflected particles contribute to the channeling efficiency evaluation. Any under- or over-estimation of either set may cause a misleading result.

4 Reconstruction method comparison

For a tracking system made of a pair of identical detector stations with an arm length Δz, the error on the angular measurement can be calculated as:

$$\sigma^2(\theta) = \frac{2\sigma_{\rm sr}^2 + \Delta z^2 \sigma(\theta_{\rm ms})^2}{\Delta z^2} = \frac{2\sigma_{\rm sr}^2}{\Delta z^2} + \sigma^2(\theta_{\rm ms}), \tag{4.1}$$

where $\sigma_{\rm sr}$ is the sensor spatial resolution and $\sigma(\theta_{\rm ms})$ is the RMS multiple scattering angular deviation in the first plane. For the H8 telescope, the effective thickness of each station is 700 µm of silicon and $\sigma_{\rm sr} \approx 7$ µm [8]. For the long upstream arm, multiple scattering dominates and the second term is the most important. At 180 GeV/c, $\sigma(\theta_{\rm ms}) \approx 5.3$ µrad.

In the case of the short downstream arm, a similar argument holds but in this case the angular error will be dominated by the spatial term. However, in estimating the angular precision on the deflected angle measurement, the two arms cannot be combined in quadrature because the multiple scattering deviations generate correlations between the planes. This can be calculated or can be estimated by Monte Carlo simulations and both methods have been applied, with excellent agreement. The Karimaki formula [11] is used, with a modification to include the contribution due to multiple scattering in the error matrix. With a long downstream arm configuration, a deflection error of ∼10 µrad should be achievable at 180 GeV/c. A simplified calculation of the error on the z-vertex reconstruction gives:

$$\sigma^2(z_{\rm int}) \approx \frac{9.4\sigma_{\rm sr}^2}{\theta_{\rm out}^2}, \tag{4.2}$$

where $\theta_{\rm out}$ is the outgoing angle to be measured, and the factor 9.4 arises using station distances in the range of the values reported in table 1. For $\theta_{\rm out} = 3$ mrad and 12 mrad the errors on the z-vertex reconstruction are $\sigma(z_{\rm int}) \approx 7.2$ mm and 1.8 mm, respectively. With a downstream arm length ≈50 cm, the error on the outgoing angle is $\sigma(\theta_{\rm out}) \approx 20$ µrad.

The two reconstruction methods (5-plane and 4-plane reconstruction) are compared in figure 3, which displays the beam divergence (a) and the tracker resolution (b) in an alignment run. The beam divergence is consistent between the two methods because the upstream arm has not been modified. With respect to the 5-plane configuration, only a slight broadening of the distribution is observed, with an increased statistical error on the $\sigma_{x'}$. Figure 3(b) illustrates clearly that the

2021 JINST 16 P05017

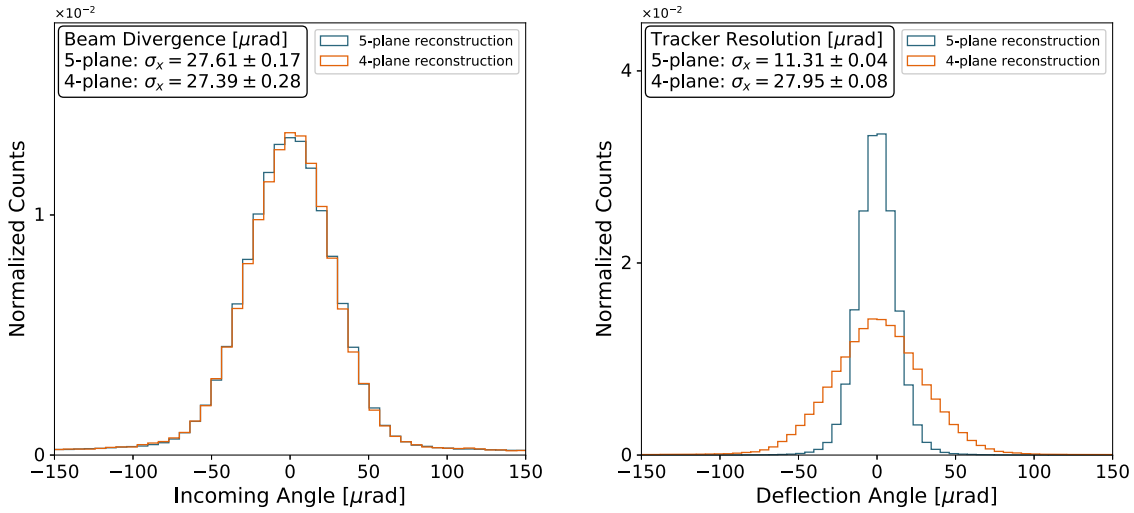

(a) Beam divergence.

(b) Tracker resolution.

Figure 3. Comparison of the four- and five-plane reconstruction methods for an alignment run. The measured horizontal divergence of the beam (a) is consistent for both reconstructions, while the resolution (b) is worsened for the four-plane configuration because of the shorter outgoing arm.

reduced length of the outgoing arm by a factor of about 30 worsens the tracker angular resolution by a factor of ≈ 2.5.

The calculated, simulated and measured performance are presented and compared for all configurations in tables 2 and 3,[2] presenting both the tracker angular and spatial resolutions. The calculated values are based on the adapted Karimaki [11] algorithm. Two different MC simulations were developed independently to give confidence that we understood small details of the tracker performance sufficiently well and allow an estimate of the uncertainties. The first method (S), is a standalone simulation of a simplified layout, that uses the same input parameters as the calculations. The second is based on the FLUKA code (F) [12, 13], where the complete layout geometry (tracker stations in air, vacuum pipes with windows and residual gas, etc.) is reconstructed. It is evident that the four-plane results are quite sensitive to the location and separation of detector stations 3 and 4, which are believed to be measured with a precision of a few mm.

5 Analysis methodology

All crystals were tested on the H8 extraction line, with a beam of secondary hadrons (protons and pions) at 180 GeV. Given the crystal length and the energy of the beam, these crystals have a curvature radius of $\approx 75.3 R_c$, $\approx 21.5 R_c$ and $\approx 35.2 R_c$,[3] respectively.

The beam divergence at the crystal position is comparable for the different cases, as shown in figure 4(a). The tracker resolution (figure 4(b)) varies because the outgoing lever arm is slightly

[2] With the five-plane reconstruction it is not possible to evaluate the transverse spatial displacement, given the constraint on the point-like interaction vertex.

[3] The critical radius for 180 GeV hadrons is $R_c \approx 0.32$ m.

2021 JINST 16 P05017

Table 2. Calculated and measured angular resolution (µrad) for the different telescope configurations with no crystal present. Monte Carlo S is a standalone simulation of a simplified layout with parameters identical to the calculations, while Monte Carlo F is based on a FLUKA model of the setup. The errors on the quantities estimated via Monte Carlo method are negligible and therefore not reported.

	Alignment	Sample 1	Sample 2	Sample 3
		Five-plane		
Calculated	9.6	9.6	9.5	9.5
Monte Carlo S	9.5	9.5	9.5	9.5
Monte Carlo F	12.2	12.0	12.1	12.0
Measured	11.3 ± 0.1	10.8 ± 0.1	11.2 ± 0.1	10.2 ± 0.1
		Four-plane		
Calculated	28.2	23.6	19.7	19.9
Monte Carlo S	28.1	23.5	19.5	19.8
Monte Carlo F	29.2	24.5	20.8	21.0
Measured	28.0 ± 0.1	23.4 ± 0.1	22.1 ± 0.1	20.4 ± 0.1

Table 3. Simulated and measured spatial resolution (µm) for the different telescope configurations with no crystal present. The errors on the quantities estimated via Monte Carlo method are negligible and therefore not reported.

	Alignment	Sample 1	Sample 2	Sample 3
		Four-plane		
Monte Carlo S	17.1	16.4	14.1	11.9
Monte Carlo F	16.7	15.8	14.5	11.8
Measured	18.50 ± 0.01	17.60 ± 0.01	16.10 ± 0.01	12.10 ± 0.01

different in each case. For sample 1 measurement, the outgoing lever arm was 44.5 cm, while it was extended to 54.7 cm and 54.1 cm for sample 2 and sample 3 measurements, respectively, by rearranging the location of the fourth station. With these arm lengths the angular resolution $\sigma(\theta_{\text{out}})$ was calculated to be 23.6 µrad, 19.7 µrad and 19.9 µrad for sample 1, sample 2 and sample 3, respectively (see table 2). For all crystals, geometrical cuts are applied to select only particles that impinge on the entry face of the crystal.

As explained in section 3, the z-vertex reconstruction produces different distributions for straight and deflected particles, as shown in figure 5 for sample 2. The channeled and dechanneled particles are considered separately from those that interact amorphously with the crystal. It is evident that a selection on z-vertex is reasonable for particles with a deflection higher than $3 \times \sigma(\theta_{\text{ms}})$, while it is not appropriate for straight particles given their broader z-vertex distribution. For deflected particles a selection $z_{\text{cut}} = [-50, 50]$ mm is applied, assuming that the crystals are mounted with their midpoints at $z = 0$, while the selection on straight particles is conceived on the basis of the MCS effects. The MCS deflection at 180 GeV/c is $\sigma_{\text{am}}(\Delta\theta_x) = 69.4$ µrad and the MCS

2021 JINST 16 P05017

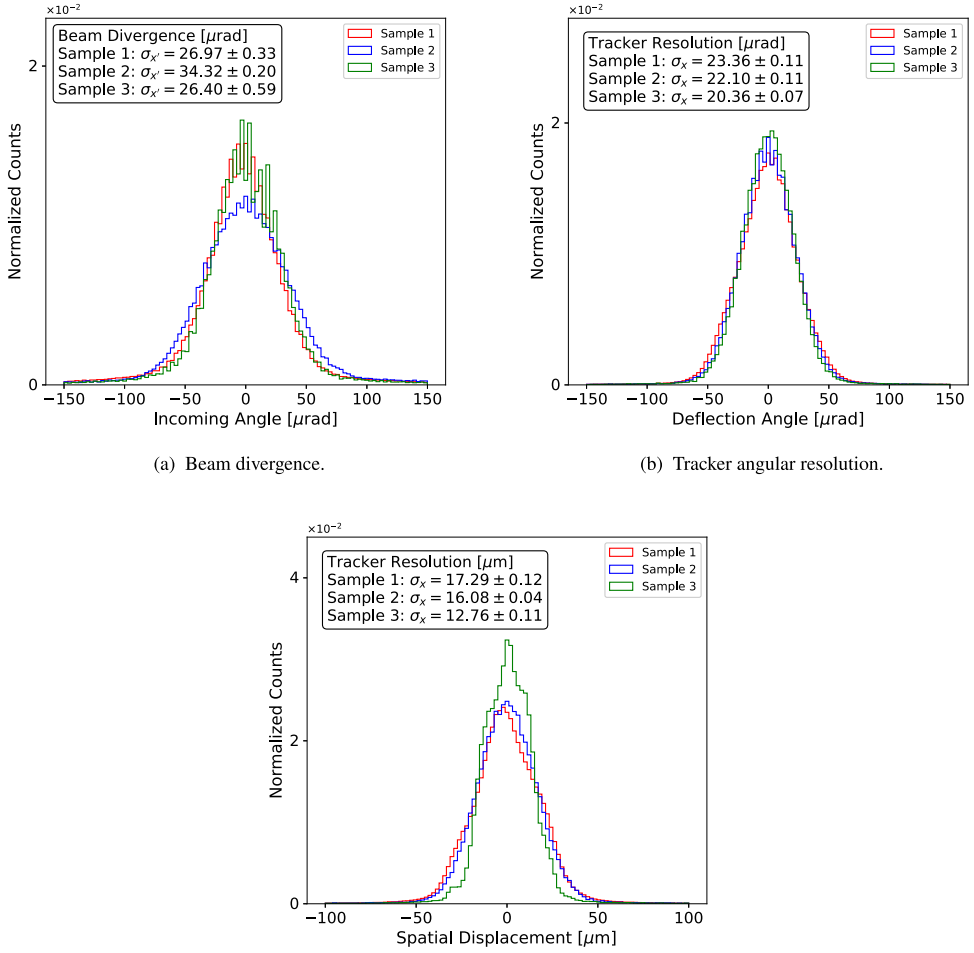

(a) Beam divergence.

(b) Tracker angular resolution.

(c) Tracker spatial resolution.

Figure 4. Beam divergence and tracker resolution (angular and spatial displacement), measured with sample 1 (red), sample 2 (blue) and sample 3 (green) during alignment runs.

displacement is $\sigma_{\text{am}}(\Delta x) = 3.2$ µm for samples 1 and 2, while for sample 3 the values are 37.1 µrad and 0.5 µm. Adding the contributions of the experimental apparatus, these values increase as reported in table 4 for calculation and Monte Carlo simulations. As one can see comparing tables 2 and 3 to table 4, the tracker contribution to the horizontal displacement Δx dominates with respect to the crystal, while the converse is true for the angular deflection $\Delta\theta_x$. These values can be identified as the angular and spatial resolution of the tracker while measuring 8 cm and 2.5 cm long crystals.

Figure 6 presents a variation analysis that evaluates the σ values of the horizontal angular deflection and spatial displacement[4] distribution, for particles that interact with the crystals in amorphous orientation; in this case sample 2 is used. The analysis is performed classifying the

[4] The horizontal displacement is measured as the difference of the horizontal impact points between the incoming and the outgoing faces of the crystals, located at $z = -40(-12.5)$ mm and at $z = +40(12.5)$ mm, for sample 1 and 2 (sample 3).

2021 JINST 16 P05017

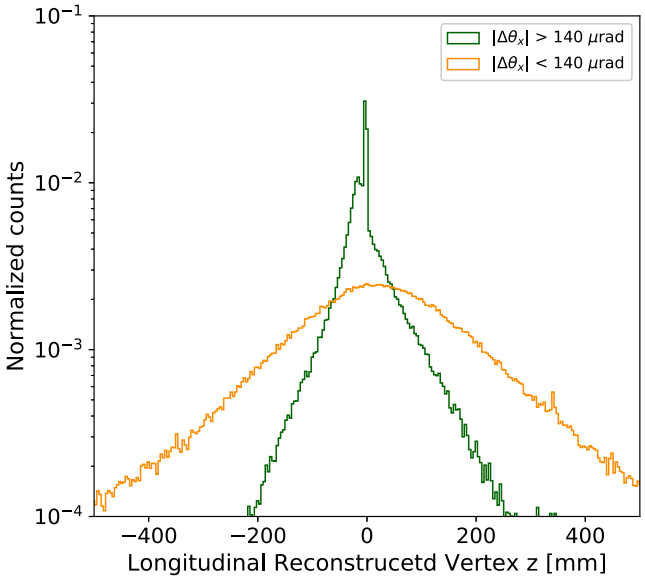

Figure 5. Longitudinal vertex reconstructed position for sample 2 crystal run. The vertex distribution is shown for tracks with a deflection larger (green) and smaller (orange) than $\approx 2 \times \sigma_{\text{am}}(\Delta\theta_x)$ in a 8 cm crystal.

Table 4. Calculated, simulated and measured resolutions for the telescope configurations with crystals present in amorphous orientation. The errors on the quantities estimated via Monte Carlo method are negligible and therefore not reported.

	Sample 1	Sample 2	Sample 3
Angular deflection (μrad)			
Calculated $\sigma(\Delta\theta_x)$	73.2	72.2	42.2
Monte Carlo S $\sigma(\Delta\theta_x)$	73.3	72.4	42.0
Monte Carlo F $\sigma(\Delta\theta_x)$	76.4	74.5	45.4
Measured $\sigma(\Delta\theta_x)$	72.2 ± 3.1	76.4 ± 1.3	43.6 ± 2.9
Spatial displacement (μm)			
Monte Carlo S $\sigma(\Delta x)$	15.9	14.3	11.7
Monte Carlo F $\sigma(\Delta x)$	16.3	14.6	12.0
Measured $\sigma(\Delta x)$	16.6 ± 0.6	15.9 ± 0.1	11.3 ± 0.1

straight tracks by different selections on the angular deflection and spatial displacement. In this case values equal to 70 μrad and 16 μm and their multiples are chosen. These values are comparable with the calculated $\sigma(\Delta\theta_x)$ and $\sigma(\Delta x)$ in table 4. The results shown in figure 6, demonstrate how the evaluation of the σ values is dependent on the cuts made on straight tracks because of tails in the distributions. It also shows how angular resolution depends on the angular selection, while the spatial resolution varies with the displacement selection.

Therefore, to select straight particles that interact with sample 2, a cut on the deflection angle of $|\Delta\theta_x| < 140$ μrad was chosen given the small contribution of the tracker. For the displacement, a selection cut $|\Delta x| < 32$ μm was applied. For the other samples, similar cuts are selected equal to

2021 JINST 16 P05017

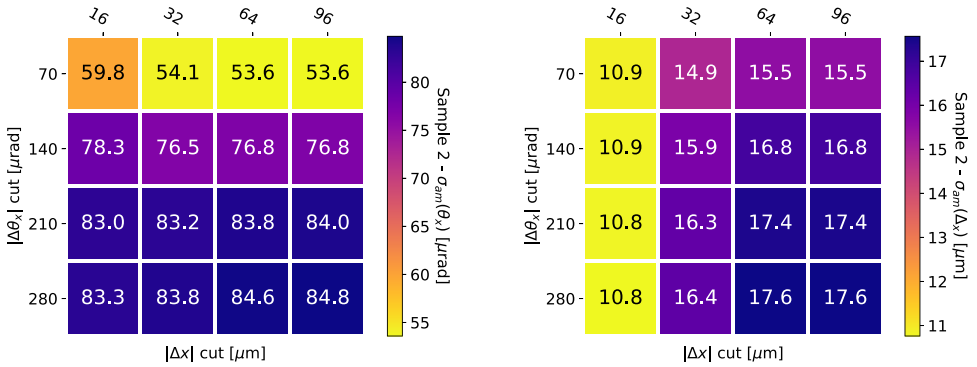

(a) Sample 2, Angular Deflection

(b) Sample 2, Spatial Displacement

Figure 6. RMS values of angular deflection and spatial displacement for particles interacting with crystals in amorphous orientation. Variation over angular and spatial selection are explained in the text. Sample 2 data are presented as an example.

Table 5. Summary of measurements for sample 1, 2 and 3. The telescope angular resolution for the measurements are reported in table 2.

	Sample 1		Sample 2		Sample 3	
Measure	$\theta_c/2$	θ_c	$\theta_c/2$	θ_c	$\theta_c/2$	θ_c
Torsion (μrad/mm)	-10.6 ± 1.3		-31.4 ± 1.4		1.6 ± 0.6	
Length (mm)	80		80		25	
CH bending (mrad)	3.33 ± 0.01	3.32 ± 0.01	11.61 ± 0.01	11.61 ± 0.01	2.22 ± 0.01	2.22 ± 0.01
CH peak σ (μrad)	24.8 ± 1.3	21.4 ± 1.2	32.3 ± 1.2*	33.7 ± 1.1*	27.8 ± 1.2	27.9 ± 1.0
η_{CH} (%)	28.3 ± 1.8	22.5 ± 1.8	16.8 ± 0.4	14.7 ± 0.4	43.8 ± 1.1	34.5 ± 0.8
AM peak σ (μrad)	72.2 ± 3.1		76.4 ± 1.3		43.6 ± 2.9	
VR peak μ (μrad)	-17.9 ± 3.7		-18.4 ± 1.8		-15.7 ± 2.4	
VR peak σ (μrad)	71.5 ± 3.7		73.0 ± 1.8		38.2 ± 2.4	

*Evaluated with vertical impact selection from 0.9 mm to 1.1 mm.

about twice the calculated $\sigma(\Delta\theta_x)$ and $\sigma(\Delta x)$, as reported in table 4. These cuts are then applied to measure the MCS deflection and displacement of particles at 180 GeV/c interacting with the samples in amorphous orientation, still reported in table 4.

6 Preliminary results

Once all the selections are applied to the data sets, a standard analysis for crystal performance [14] is executed.

Estimates of crystal torsion are reported in table 5. The torsion is measured as the linear correlation between the mean deflection angle and the vertical impact parameter and is used to correct the impact angle. The large torsion of sample 2 is the main cause of the larger σ_{CH} with respect to the other crystals. In table 5 this value is evaluated with a very narrow selection

2021 JINST 16 P05017

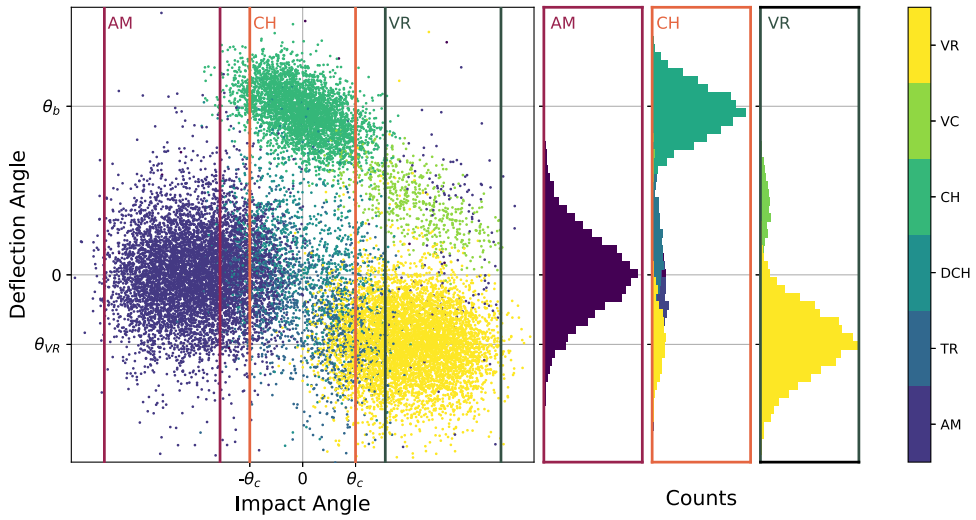

Figure 7. Deflection as a function of impact angle of particles interacting with a bent crystal of bending θ_b. The effect experienced by each track is coded by the color bar on the right. All the coherent phenomena that arise in a bent crystal oriented in planar channeling are listed: amorphous interaction (AM), transition region (TR), planar channeling (CH), dechanneling (DCH), volume capture (VC) and volume reflection (VR). The deflection distributions on the right are produced selecting tracks by their impact angle. For angles lower than θ_c the AM distribution (purple solid lines) is obtained, showing a distribution centered on 0; for impact angle between θ_c (or $\theta_c/2$) the CH distribution (orange solid lines) is obtained, showing the channeled particles deflected by an angle θ_b; for impact angle higher than θ_c the VR distribution (green solid lines) is obtained, showing the reflected particle peak around θ_{VR} (opposite sign with respect to θ_b).

on the vertical impact parameter, which gives results closer to the range observed with other samples.

The deflection distributions needed to measure the channeling and other observable phenomena are obtained by selecting tracks according to their impact angle. Figure 7 shows a schematic of the correlation between the deflection and the impact angle of positively charged particles in a bent crystal. Selecting tracks by their impact angle and generating the deflection distribution allows studying different phenomena. By selecting tracks with an impact angle within θ_c[5] (or $\theta_c/2$) one can obtain the deflection distributions in figure 8.[6] These channeling distributions are used to evaluate the channeling bending angle and the channeling efficiency with a Gaussian fit of the channeling peak. The channeling efficiency is evaluated as twice the integral of the upper side of the channeling peak divided by the total number of selected events:

$$\eta(\theta_{\rm sel}) = \frac{2 \times N_{\rm CH}\left[\mu_{\rm CH}, \mu_{\rm CH} + 3 \times \sigma_{\rm CH}\right]}{N_{\rm tot}}, \tag{6.1}$$

where $\theta_{\rm sel}$ is chosen to be the critical angle (or half the critical angle). To estimate the error on the efficiency evaluation, both the statistical errors on the channeling peak parameters $\delta\mu_{\rm CH}$ and

[5] The critical angle for 180 GeV hadrons is $\theta_c \approx 16$ µrad.

[6] Particles with impact angles below θ_c are the only ones that could undergo channeling. It would not be useful to account for particles that do not have the right parameters to be channeled in the first place. The $\theta_c/2$ distribution is instead used to reduce the tail effect of the impact distribution and look at efficiency in the bulk of the crystal channel.

2021 JINST 16 P05017

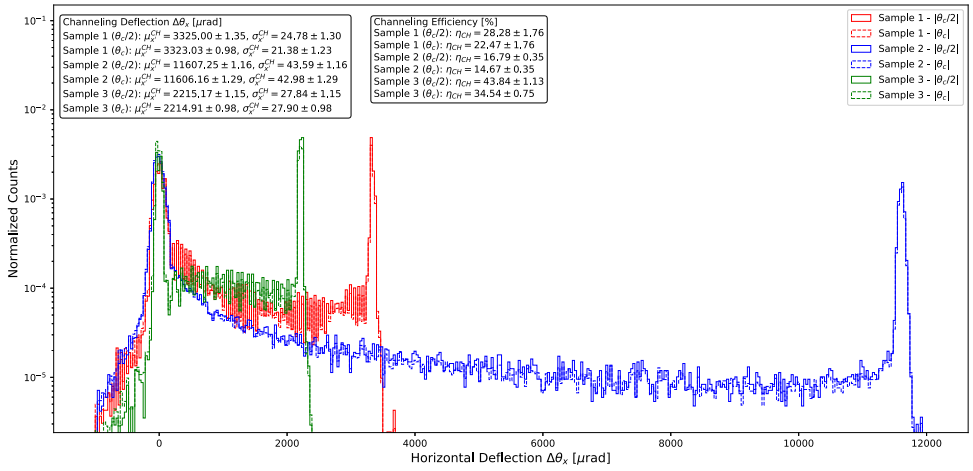

Figure 8. Deflection distribution for sample 1 (red) and sample 2 (blue), with incoming angle selection of θ_c (solid) and $\theta_c/2$ (dashed). The legends on the plot summarise the results. Channeling peak parameters are presented in the left box while channeling efficiencies are presented in the central one.

$\delta\sigma_{CH}$ are taken into account and used to change the integral limits in eq. (6.1) as:

$$N_{CH}^{\pm} = N_{CH}[\mu_{CH} \pm \delta\mu_{CH}, \mu_{CH} \pm \delta\mu_{CH} + 3 \times (\sigma_{CH} \mp \delta\sigma_{CH})]. \tag{6.2}$$

In this way, one can obtain the maximum overestimation and minimum underestimation on the number of channeled particles. The half-difference between the minimum and maximum value of the efficiencies obtained is used as the efficiency error. The results are reported in table 5 and shown in figure 8.

The regions of Volume Reflection (VR) and amorphous (AM) orientation are selected as tracks with impact angles that are larger and smaller than the critical angle, respectively, as illustrated in figure 7. The corresponding deflection distributions provide information about the AM and VR peaks, useful parameters to check the quality of the analysis. The values obtained are reported in table 5 and are consistent with previous measurements of VR deflection with a beam of 180 GeV energy.

7 Conclusions

Crystals of several cm in length with a bending angle of a few mrad were measured with the UA9 experimental apparatus in the CERN North Area for the first time. A dedicated track reconstruction method was developed to measure the crystal properties, which takes advantage of a consistent treatment of both large and small deflection tracks. Its robustness was compared with MCS effects and coherent crystal interactions (both channeling and volume reflection). The efficiency of the crystals measured in this work is compatible with previous measurements performed in the 1990s [7], while the measurement precision is quite improved. In particular, considering the respective crystal characteristics (length and bending angle) and the different beam energies, the efficiency measured in this work is consistent with the dependency on the ratio R/R_c [6], and with improved accuracy.

2021 JINST 16 P05017

In future measurement and test, a number of interesting results can be obtained by deploying the methodology developed in the present work.

Acknowledgments

The authors want to thanks the UA9 collaboration for the access to the data, and hope that the method developed would be useful for future detailed measurements. The crystal samples were supplied by the members of the collaboration V. Guidi and A. Mazzolari (INFN Ferrara), and the co-author W.S. Imperial College gratefully acknowledges financial support from the UK Science and Technology Facilities Council.

References

[1] V.M. Biryukov, Y.A. Chesnokov and V.I. Kotov, *Crystal Channeling and Its Application at High-Energy Accelerators*, Springer Science & Business Media, (2013).

[2] W. Scandale et al., *Observation of channeling for 6500 GeV/c protons in the crystal assisted collimation setup for LHC, Phys. Lett.* B **758** (2016) 129.

[3] S.J. Brodsky, F. Fleuret, C. Hadjidakis and J.P. Lansberg, *Physics opportunities of a fixed-target experiment using LHC beams, Phys. Rept.* **522** (2013) 239.

[4] L. Massacrier et al., *Physics perspectives with AFTER@LHC (a fixed target experiment at LHC), EPJ Web Conf.* **171** (2018) 10001.

[5] W. Scandale et al., *Observation of strong leakage reduction in crystal assisted collimation of the SPS beam, Phys. Lett.* B **748** (2015) 451.

[6] E. Bagli et al., *Steering efficiency of a ultrarelativistic proton beam in a thin bent crystal, Eur. Phys. J.* C **74** (2014) 2740.

[7] K. Elsener et al., *High efficiency beam deflection by planar channeling in bent silicon crystals, Proceedings of International Conference on Particle Accelerators.* Vol. 2 (1993), p. 1363.

[8] M. Pesaresi et al., *Design and performance of a high rate, high angular resolution beam telescope used for crystal channeling studies,* 2011 *JINST* **6** P04006.

[9] G. Hall, G. Auzinger, J. Borg, T. James, M. Pesaresi and M. Raymond, *A high angular resolution silicon microstrip telescope for crystal channeling studies, Nucl. Instrum. Meth.* **924** (2019) 394.

[10] G. Hall, T. James and M. Pesaresi, *Optimisation of a silicon microstrip telescope for UA9 crystal channeling studies,* 2020 *JINST* **15** C05014.

[11] V. Karimäki, *Explicit covariance matrix for particle measurement precision, Nucl. Instrum. Meth.* **410** (1998) 284.

[12] T.T. Böhlen et al., *The fluka code: developments and challenges for high energy and medical applications, Nucl. Data Sheets* **120** (2014) 211.

[13] G. Battistoni et al., *Overview of the fluka code, Ann. Nucl. Energy* **82** (2015) 10.

[14] R. Rossi, G. Cavoto, D. Mirarchi, S. Redaelli and W. Scandale, *Measurements of coherent interactions of 400 GeV protons in silicon bent crystals, Nucl. Instrum. Meth.* **355** (2015) 369.

2021 JINST 16 P05017